CONTENTS

Fatigue crack growth of two pipeline steels in a pressurized hydrogen environment ☆

Andrew J. Slifka *, Elizabeth S. Drexler, Nicholas E. Nanninga, Yaakov S. Levy, J. David McColskey, Robert L. Amaro, April E. Stevenson

NIST, Materials Reliability Division, 325 Broadway, Boulder, CO 80305, USA

ABSTRACT

Fatigue crack growth tests were conducted on two pipeline steel alloys, API 5L X52 and X100. Baseline tests were conducted in air, and those results were compared with tests conducted in pressurized hydrogen gas. All tests were run at (load ratio) $R = 0.5$ and a frequency of 1 Hz, except for one test on X100, run at 0.1 Hz. Tests were conducted at hydrogen pressures of 1.7 MPa, 7 MPa, 21 MPa, and 48 MPa. Fatigue crack growth rates for both X100 and X52 were significantly higher in a pressurized hydrogen environment than in air. This enhanced growth rate appears to correlate to pressure for X100 but may not for X52.

Published by Elsevier Ltd.

1. Introduction

The use of hydrogen as a fuel and as an energy carrier is likely to increase in the next decade. According to the Fuel Cell and Hydrogen Energy Association, "Nearly all of the major auto manufacturers have 2015 as the projected release date for mass-produced models" [1], which means that economical transportation and distribution of hydrogen is needed prior to 2015. Hydrogen can be electrolyzed with excess electricity generated by solar and wind farms. The hydrogen can be stored and used during peak demand or transported to areas of need for Smart Grid applications. According to the U.S. Department of Transportation, "Pipelines are the safest and most cost-effective means to transport the extraordinary volumes of natural gas and hazardous liquid products that fuel our economy" [2]. Therefore, one would expect that pipelines would be the safest and most economical means of transporting large volumes of hydrogen. The primary issue with hydrogen is that it embrittles most materials, leading to a likely decrease in lifetime of a pipeline transporting hydrogen, compared to the transport of natural gas. The embrittlement of pipeline steels due to hydrogen is well documented in the case of tensile tests [3–17]. However, the literature contains far less information on hydrogen-assisted cracking or fatigue properties of pipeline steels [3–5,12,13,18–22]. There has been some recent work done on fatigue crack initiation with a 3-point bend test, but little work

on fatigue crack growth in pipeline steels [23,24]. Some work has been done in recent years on measurement of fatigue properties of X60, X70 and X80 pipeline steels [8,13,20].

In order to safely and efficiently design pipelines for transport of hydrogen gas, codes such as ASME B31.12 on Hydrogen Piping and Pipelines are used [25]. Due to the dearth of fatigue information, codes rely upon tensile data in order to factor in design variables such as pressure. However, pipelines are not operated at or near material yield stress, such that embrittlement data from tensile tests may produce codes that are too conservative. Since safety is the primary factor in these codes, fatigue data from many different pipeline steels, encompassing many different microstructures, is needed if any modifications are to be made to the codes. These pipelines are expected to operate for decades, which will allow many or most of the hydrogen traps in the steel to be filled. This work will not address that issue. Future work is planned on samples that have been pre-charged either with high-pressure gas at elevated temperature or by cathodic charging. However, due to the rapid rate of diffusion of hydrogen in ferritic steels [26], being at least 5 orders of magnitude greater than in austenitic steels [6,27], hydrogen diffuses the few mm to the midpoint of a pipeline steel section in a manner of minutes [26]. An additional effect that is not accounted for in the results presented in this work is that of very slow stress cycling. A fuel pipeline would be expected to experience pressure cycles on the order of two per day. That type of slow cycling, done over some breadth of stress intensity ranges, would take a prohibitive amount of time to complete. However, some work has been done in air at very low cyclic frequencies [28]. That work includes fatigue crack growth rate (FCGR) measurements down to 0.001 Hz. Those authors

demonstrate that low temperature creep blunts the crack tip and reduces the crack growth rate. That phenomenon would work against the corrosion fatigue effect of hydrogen at the crack tip. Moreover, the strain hardening differences between X52 and X100 could cause a significant difference in creep behavior, because strain hardening effects can cause large differences in creep behavior of pipeline steels [29]. Measurements in hydrogen at very low cyclic loading rates need to be done to resolve the relationship between these competing mechanisms.

The work presented here deals only with diffusible hydrogen in the lattice that is near the crack tip. It reports measurements of FCGR of X52 and X100 pipeline steels at 1 Hz loading frequency, which is high compared to what an actual pipeline would see. These steels were chosen because X52 is material that is currently being used for hydrogen pipeline applications, and X100 represents the upper limit of strength that is likely to be used in the near future. The microstructures of these steels are very different, which may lead to differences in FCGR.

2. Materials and methods

2.1. The materials

This study investigates the fatigue crack growth properties of two very different grades of linepipe material, API 5L types X52 and X100. Sections of pipe were supplied from members of the pipeline industry. The X52 pipe was 0.51 m diameter and 12.7 mm thick and the X100 pipe was 1.3 m in diameter and 20.6 mm thick. The X100 pipe was an experimental pipe produced in the latter half of the 1990s. The X52 pipe was of early 21st century vintage and had never been in service.

Round specimens were made according to ASTM E8 [30] and were tested in air with a strain rate of 3×10^{-3} mm/s. The material was not flattened prior to machining the tensile specimens in order to measure the properties of the formed pipe. The tensile properties of the base material from each pipe are shown in Table 1. The "L" orientation, longitudinal, is along the pipe axis, and the "T" orientation, transverse, is along the hoop direction, perpendicular to the longitudinal direction.

As would be expected with materials with such different strengths, the microstructure was very different when comparing the two pipes. The X52 has about 10% pearlite in a polygonal ferrite microstructure, shown in Fig. 1a. This material shows some banding, but none of large scale, but shows a small amount of chemical segregation at low magnification, seen in Fig. 1a. Fig. 1b shows a higher-magnification optical image of the microstructure, which is predominantly polygonal ferrite plus carbide. The X100 material is shown in Fig. 2 at two magnifications. The low-magnification image shows that this material has considerable banding or macroscopic chemical desegregation, but it is not concentrated at any particular level through the thickness. The high-magnification image shows a fine-grained microstructure of lath-like components, including bainite and acicular ferrite. The small-scale banding, or chemical microsegregation, is evident even at high magnifications. Table 2 gives the chemical compositions of these two steels.

Table 1
Tensile properties of the base metals X52 and X100 used in this study.

Steel	Orient.	σ_y (MPa)	σ_{UTS} (MPa)	e_f (%)
X52	L	426 ± 10	491 ± 8	27.4
X52	T	436 ± 5	504 ± 5	27.0
X100	L	705 ± 40	803 ± 6	20.3
X100	T	794 ± 11	827 ± 5	19.3

2.2. The test matrix

Material from each linepipe was used to measure the FCGR in air, at various pressures of hydrogen gas, and at different frequencies. The X52 was tested at two different hydrogen pressures (7 MPa and 21 MPa); in addition to those pressures, the X100 material was also tested at 1.7 MPa. Only the X100 material was tested at different frequencies: 1 and 0.1 Hz. One specimen was tested for each condition.

The sub-sized specimens were designed according to the specifications for a compact tension (CT) specimen, found in ASTM E647-05 [31], with a W = 26.4 mm. Fig. 3 shows a drawing with the pertinent dimensions of the CT specimens. The surface roughness R_a was less than 0.25 µm for all specimens tested. The specimens are made in the *T–L* orientation, which means that the crack runs in the longitudinal (along the pipe axis) direction of the pipeline, and the cyclic loading is applied in the transverse (or hoop stress) direction, in accordance with ASTM E399 [32]. A fatigue crack is most likely to propagate in the longitudinal direction of a pipe due to the effect of the higher stress in the transverse, or hoop, direction.

The specimens were fatigue precracked (FPC) in air to generate a sharp crack at the notch tip with a load ratio R = 0.1 and a frequency of 10 Hz. The average length of the precrack was 3.12 mm, which corresponds to the width of the notch.

2.3. Pressurizing system

Specimens were tested in a stainless-steel pressure vessel (internal diameter 101.6 mm diameter and length 254 mm), capable of holding hydrogen gas pressures up to 140 MPa. The pressure vessel was closed on one end and had a sliding seal and pull rod on the opposite end. The pull rod was connected to the actuator of a servo-hydraulic test frame with 90 kN loading capacity. Fig. 4 provides a schematic of the test frame, pressure vessel, fatigue sample, and instrumentation used for testing. An internal load cell, designed for use in high-pressure hydrogen gas, was employed inside the pressure vessel. This was done because friction forces at the sliding seals, which vary with test pressure, can lead to differences between the force measured at the externally-mounted load cell on the test frame and that which would be exerted on the specimen, as seen in Fig. 5. The internal load cell uses a linear variable differential transducer to measure displacement, and was calibrated in air using the external load cell as a reference. All reported forces are those measured from the internal load cell. Control of cyclic loading was done with the internal load cell in the form of a sine wave, plotted in black in Fig. 5. Crack length was determined by compliance [$\Delta v / \Delta P$, where v = CMOD (crack mouth opening displacement) and P = force], as measured by a clip gauge tracking the CMOD. A relationship that uses the elastic modulus of the material, the geometry of the specimen, and the CMOD is used to calculate crack length, per ASTM E647-05 [31].

Upon installation and sealing the pressure vessel, the chamber was purged twice with ultra-pure helium (99.9999%) and three times with ultra-pure hydrogen (99.9995%) to 14 MPa, or the designated test pressure, whichever was lower, before the final pressurization to the test pressure. This entire purging/venting process is controlled by a computer program which automatically opens and closes air-operated valves in a pre-determined sequence to effect the cleansing of the system. Automating the cleansing and maintaining pressure eliminates the risk of human error and provides consistency from run to run.

This series of tests were conducted with hydrogen that was generated on-site with an electrolyzer unit. Analysis of the gas produced showed that it was at least as clean as the purest
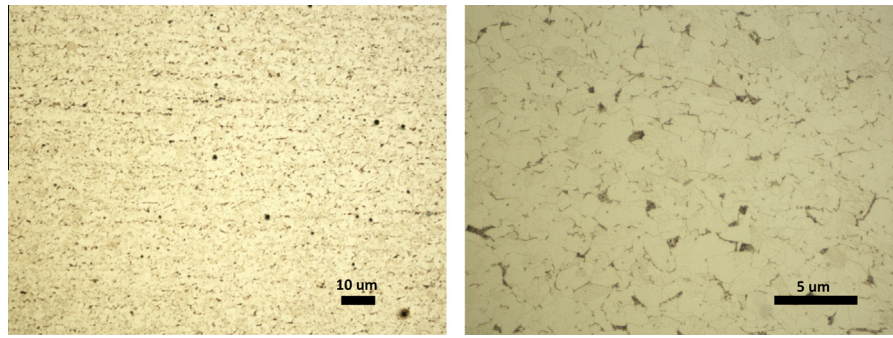
Fig. 1. Low-magnification (left) view of X52 material, showing slight chemical desegregation in the longitudinal pipe direction, and (right) at higher magnification showing the polygonal ferrite and pearlite microstructure.

(A)   **(B)**
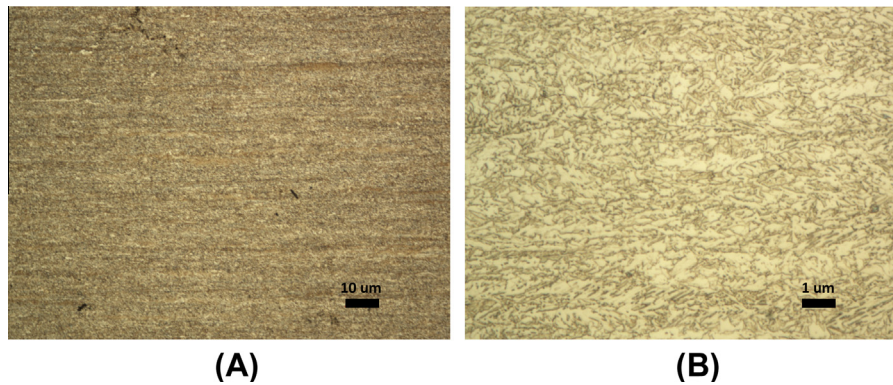
Fig. 2. X100 pipeline steel at 25× (A) and 250× (B), showing no large-scale chemical segregation, but chemical microsegregation in the longitudinal pipe direction.

Table 2
Chemical compositions of the two pipeline steels used in this study.

Alloy	Chemical composition (wt%)								
	C	Mn	Si	S	P	Ni	Cr	Mo	Nb + V + Ti
X52	0.060	0.870	0.120	0.006	0.011	0.020	0.030	–	0.030
X100	0.064	1.870	0.099	<0.001	0.009	0.470	0.023	0.230	0.036
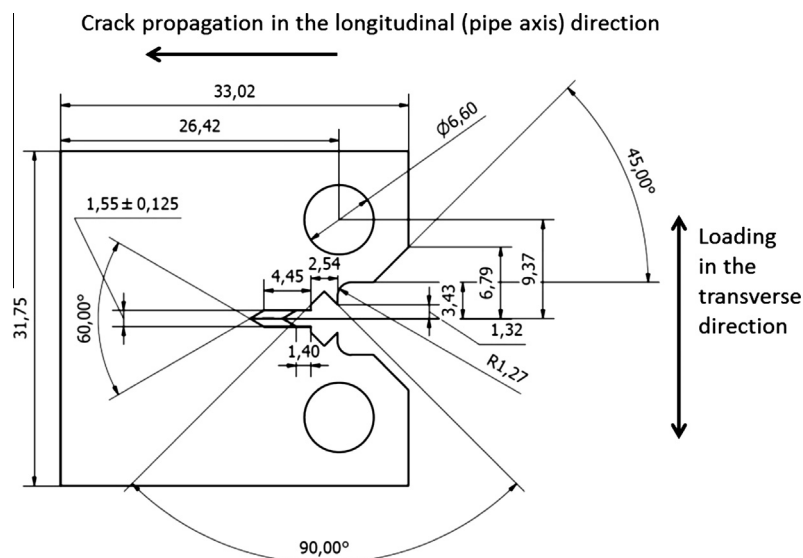
Fig. 3. Diagram of the compact tension specimen used for the tests of the rate of fatigue crack growth. All dimensions are in mm.
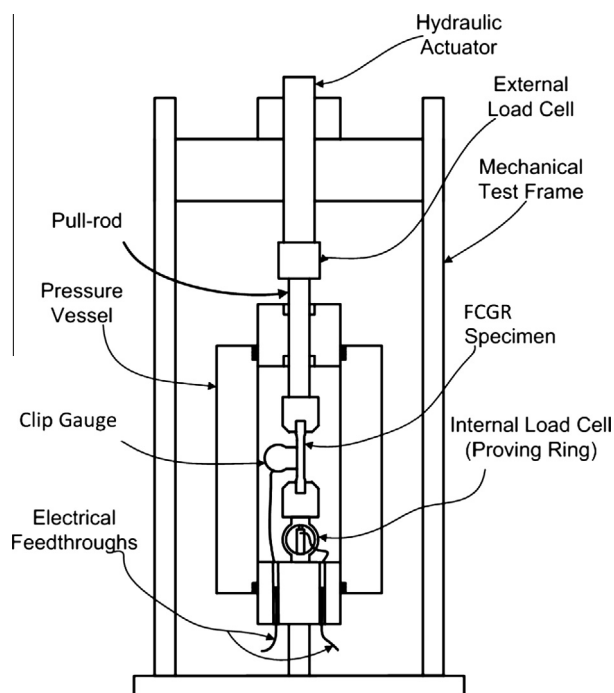
Fig. 4. Schematic of the hydrogen pressure vessel and mechanical testing apparatus showing the salient parts of the device.

hydrogen gas available for purchase. Table 3 shows gas purity of commercial ultra-high-purity product before running through a gas supply system and our on-site-generated gas after running through a gas supply system.

2.4. Fatigue crack growth rate testing

Tests were conducted according to ASTM E647-05 [31] with a load ratio, R, of 0.5 and in load control. The set loads were controlled from the internal load cell. An MTS[1] load frame capable of producing 100 kN load was used, as well as MTS Fatigue and Fracture V 4.11A [1] software that continuously calculated and recorded crack growth every 0.04 mm. Values for K and ΔK were also calculated within the program and were based upon the geometry of the specimen, the force, the compliance (ratio of CMOD to force), and the Young's modulus and yield strength of the material. The test was concluded when the program calculated the crack length to be approximately 2/3 the length of the gage section (17 mm in the W direction). The general uncertainty of fatigue measurement is given in ASTM E647-05 [31] and is ±32% for da/dN and ±9% for ΔK. The data were reduced by use of a five point average of the values given from the 0.04 mm crack length interval.

There is no pre-charging done for these fatigue tests. The steels have not been subjected to hydrogen in a pipeline application, and before testing, chemical analysis of the X100 pipe material showed 0.0006% H in the sample. The manufacturer of the X52 steel did not test for hydrogen as part of their chemical analysis. Each specimen experienced short exposures to hydrogen gas pressure, shown above as part of the *Pressurizing System*. The fatigue test was started shortly after the final hydrogen pressurization, resulting in hydrogen exposure of less than 3 h prior to fatigue. Each test
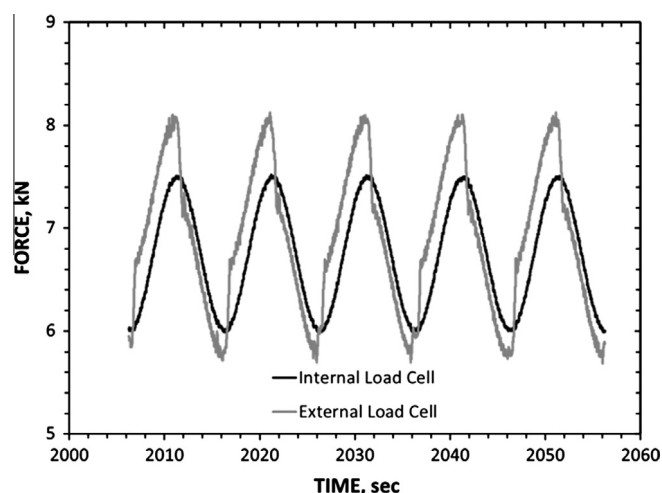
---

[1] Commercial equipment, instruments, or materials are identified only in order to adequately specify certain procedures. In no case does such identification imply recommendation or endorsement by the National Institute of Standards and Technology, nor does it imply that the products identified are necessarily the best available for the purpose.

Fig. 5. Force plot showing the difference in the force measured by the internal load cell (black) and the external load cell (gray) during cyclic loading at a chamber pressure of 14 MPa.

at a loading frequency of 1 Hz ran for 3–7 days to completion, and the 0.1 Hz test ran for 21 days. At room temperature and the test pressures used, it was not thought that traps in the microstructure would be filled and that the hydrogen-environment-assisted-corrosion effect was due primarily to diffusible hydrogen in the lattice. Since the diffusible hydrogen migrates out of the specimen in less than an hour, hydrogen content was not measured after testing.

3. Results

Fig. 6 shows the results of fatigue crack growth on all the specimens tested at 1 Hz for this study; the results are displayed as the change in crack length per change in cycle versus the range of the stress intensity factor (da/dN versus ΔK). FCGR data from the X52 alloy, measured by Sandia National Laboratories at a hydrogen gas pressure of 21 MPa, R = 0.5, and 1 Hz is shown for comparison [33]. Data is shown for tests conducted on the X100 material in air and at hydrogen gas pressures of 1.7 MPa, 6.9 MPa, and 20.7 MPa. The data show that in general there is an increase in FCGR at a given ΔK with respect to increasing hydrogen gas pressure. This correlation between hydrogen gas pressure and FCGR appears less strong, if at all, for the X52 data, as seen in Fig. 7. Data from Sandia on a similar material are included for comparison [33]. For practical purposes, hydrogen embrittlement occurs locally at the crack tip process zone on a per-cycle basis, causing the increased rate of crack growth over that in air. The three prevailing theories of damage mechanisms due to hydrogen concentration within a material are hydrogen enhanced decohesion (HEDE), hydrogen enhanced localized plasticity (HELP), and adsorption induced dislocation emission, all of which are discussed in [35]. A detailed explanation of potential mechanisms for this increase can be found in [34], as well as a model of this X100 FCGR data.

Two X100 specimens were fatigued at different frequencies. Fig. 8 shows this comparison. It can be observed that the slower the rate of fatigue the higher the FCGR at a given ΔK, above a ΔK of 12 MPa m$^{1/2}$. The effect of lowering the frequency appears to be similar to raising the gas pressure. The FCGR model of this data shows this to be true quantitatively [34].

The datasets from both materials display a distinct knee from a larger to a smaller slope in the da/dN curves at values for ΔK between 11 MPa m$^{1/2}$ and 15 MPa m$^{1/2}$ that is not associated with the transition from Stage I to Stage II fatigue behavior. Rather, this

Table 3
Comparison of gas purity from a commercial supplier and product generated with an electrolyzer.

Specimen	Gas cylinder purging process	Species (ppm)									
		O_2	H_2O	CO	CO_2	N_2	N_2O	Ar	CH_4	Hydrocarbons	H_2
Bottle	N/A	<0.05	<0.05	<0.02	<0.02	<0.2	–	–	<0.01	–	99.9999
NIST-SG[a]	Purge and evacuate	<0.5	<1.0	<0.1	<0.1	<1.0	<0.1	<1.0	–	<0.1	99.9999

[a] NIST-SG is self-generated hydrogen – run through system but not chamber.
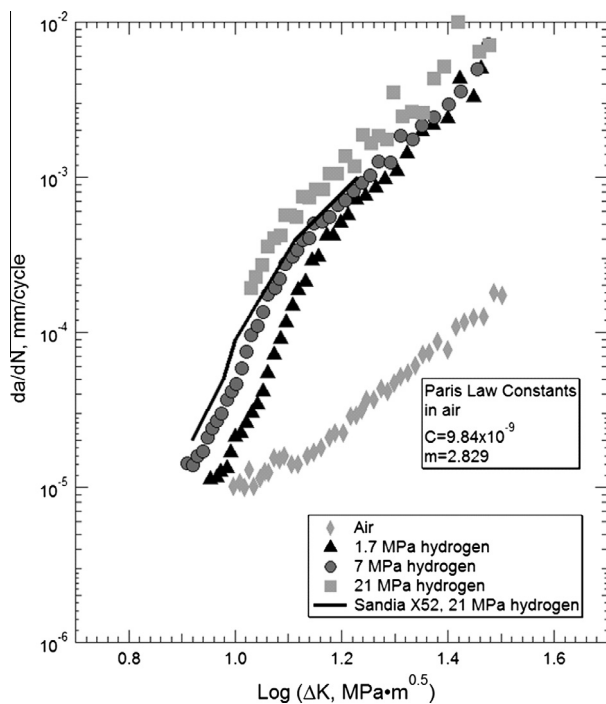

Fig. 6. Fatigue crack growth rate data for X100 steel, comparing results in air with that in pressurized hydrogen gas. The dotted line shows results from an X52 alloy measured at Sandia National Laboratories [33]. Paris law constants given for X100 in air.
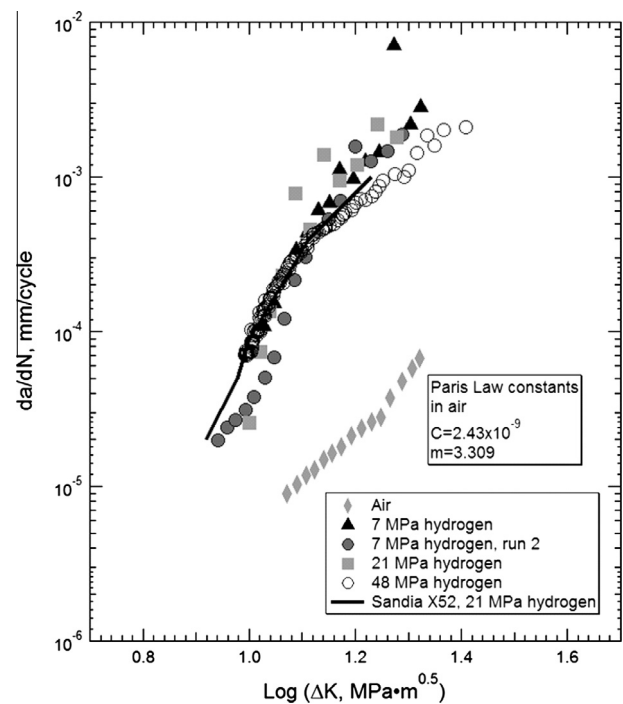

Fig. 7. Fatigue crack growth rate data for X52 in air and at various hydrogen gas pressures, including comparative data at 20.7 MPa from Sandia National Laboratories [33]. Two specimens were run at 6.9 MPa. Paris law constants given for X52 in air.

knee appears to be associated with the transition from mostly intergranular to mostly transgranular crack growth within Stage II as stress intensity increases, which has been noted by other authors [5,36,37]. The low-ΔK region will be referred to as the transient region, and the high-ΔK region will be called the steady-state region. Fig. 9 shows the precrack, the transient region (low ΔK), and the steady-state region ($\Delta K > 15$ MPa m$^{1/2}$), which can be observed on the fracture surface.

4. Fractography

Representative scanning electron microscope (SEM) micrographs of X100 fatigue crack propagation surfaces are shown in Figs. 9 and 10.

The micrographs in Figs. 9 and 10 indicate that the morphology of the specimen's fracture surface transitioned from a mixed transgranular–intergranular character during precracking in air to mixed intergranular fracture with planar fracture and fatigue striations during transient FCG, characterized by low ΔK values and shown in Fig. 10(b). However, the steady-state regime is dominated by transgranular FCG with considerable crack branching. These findings are consistent with those of [5,37]. Additionally, fracture surfaces were scanned with a commercially available stylus profilometer that has a contact tip radius of 2.5 μm and a

resolution of 15 Å. A representative plot of fracture surface height versus distance is shown in Fig. 11. The length of the crack, measured from the specimen shown in Fig. 9, correlates with the crack length that corresponds to the ΔK at the knee, or transition seen in the slopes of the FCGR curves.

The fatigue crack propagation surface of X100 steel tested in hydrogen exhibits three regimes of surface asperities, depending upon the FCGR: (1) the precrack region, (2) the transient regime exhibiting the lowest surface roughness ($Ra = 2.2$ μm), and (3) the steady-state regime, which has a larger surface roughness ($Ra = 4.7$ μm). The transient regime is dominated by the crack growth within the volume where the concentration of hydrogen is maximized within the process zone, whereas within the steady-state regime the crack growth per cycle extends beyond this hydrogen-concentrated region.

5. Discussion

The data show a clear distinction between those specimens tested in air and those in a hydrogen gas environment. In particular, the specimens tested in hydrogen gas exhibit a higher slope of FCGR at values of $\Delta K < 14$ MPa m$^{1/2}$. This increase results in FCGR values 1–1.5 orders of magnitude higher. This effect is observed when testing at hydrogen pressures as low and as high
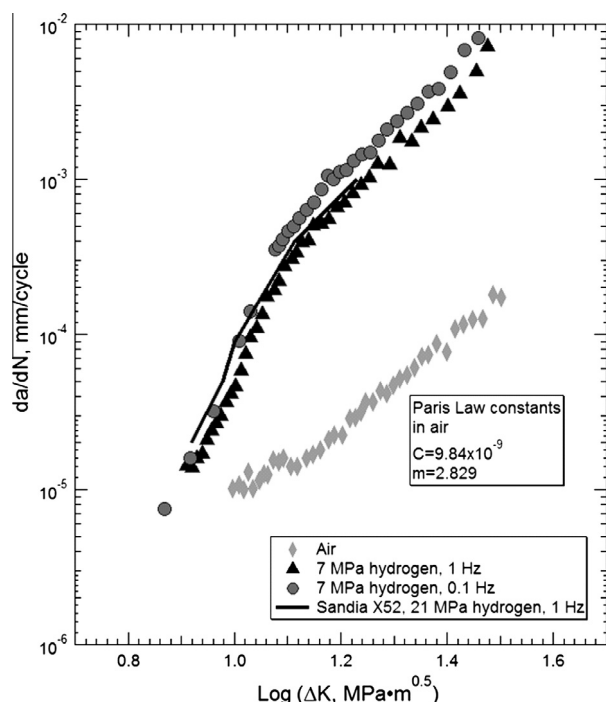
Fig. 8. Fatigue crack growth rate data for X100 at 7 MPa and loading frequencies of 1 Hz and 0.1 Hz, including comparative data (1 Hz) at 20.7 MPa from Sandia National Laboratories [33]. Paris law constants given for X100 in air.
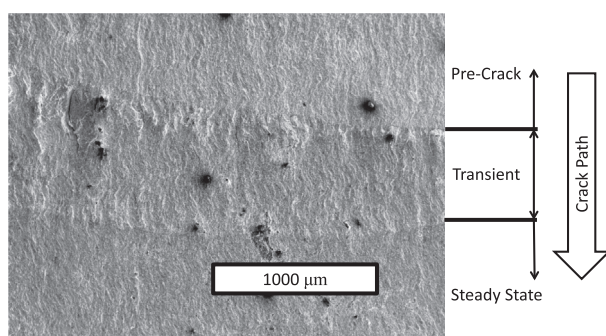

Fig. 9. Fatigue surface of X100 Steel tested in 20.7 MPa hydrogen showing different character as the crack moves from precrack to the transient region and to the steady-state region.

as 1.7 MPa and 48 MPa, respectively. At higher values of ΔK the slope decreases, more closely resembling that of data acquired in air. The authors believe that the length of the crack growth per cycle plays a critical role in this phenomenon. At smaller values of da/dN the crack is growing within a region characterized by stress-enhanced hydrogen diffusion, ranging from 250 nm to 450 nm, yet within the crack-tip-process zone defined by the stress intensity. However, at larger values of da/dN, the per-cycle crack growth outpaces the area affected by stress-assisted hydrogen diffusion, thus it more closely behaves as a test would in air added to a maximum length of hydrogen-diffusion-affected growth [38–43]. The change in slope occurs at higher values of da/dN and lower values of ΔK as the pressure increases. This would imply that the effect of hydrogen increases and perhaps the volume of material near the crack tip where hydrogen accumulates is larger at higher pressures. The effect of hydrogen concentration at the crack tip as a function of hydrogen embrittlement, loading, specimen thickness, and fatigue crack

growth can be found in numerous sources [15,16,34,44,45]. The effect of stress-assisted hydrogen concentration on fatigue crack growth per cycle follows directly from that on hydrogen embrittlement. At low values of ΔK, cracking in fatigue would be expected to be similar to that of very slow strain rate ($<10^{-6}$ mm/s) tensile testing. As the value of ΔK increases, the character of the per-cycle cracking in fatigue would resemble hydrogen embrittlement at decreasing values of strain rate.

Fig. 12 illustrates the crack extension to stress-assisted hydrogen concentration interactions for both X100 and X52 steels. The figure shows the normalized stress-assisted hydrogen concentration versus distance in front of the crack tip. In this way ambient hydrogen pressure and material-specific values of hydrogen-concentration activation energy are disregarded. The figure indicates the region of increased hydrogen concentration resulting from the crack tip stress field, the associated X100 and X52 yield values as well as the estimate of the fatigue process zone size for each material when the applied stress concentration factor is $\Delta K = 13$ MPa m$^{1/2}$. Given that Fig. 12 represents a snapshot in time, specifically for a particular value of ΔK, the normalized stress-assisted hydrogen concentration profile is identical for both materials. However, the material-specific yielding and the subsequent stress-redistribution will affect the peak stress-assisted hydrogen concentration within that particular steel, as shown in the figure. Fig. 12 indicates that the HA_FCG response would transition from a high slope to a lower slope when the crack extension per cycle reaches 110–380 nm for X52 and X100, respectively. Experimental results fall within this range for both materials.

Looking more closely at the X100 data, for a given value of ΔK, and at moderate values of ΔK, the crack growth rate per cycle increases with increasing hydrogen pressure. The behavior of the X52 material with respect to hydrogen pressure is not as clear as that of the X100 data. It is not known whether this lack of pressure sensitivity is due to something intrinsic to the X52 material relative to that of X100, such as a balance between crack growth per cycle, grain size, and density and type of hydrogen traps. These materials have differences in chemical compositions, and especially in microstructure. Furthermore, a third pressurized hydrogen test was conducted on X52 that used the same MTS Fatigue and Fracture[1] software with a slower (larger crack length increment) data acquisition rate, and a constant $\Delta P = 2.3$ kN, 1 Hz loading rate, and $R = 0.5$. This test, shown in Fig. 7, was conducted with the hydrogen pressurized to 48 MPa. This data may have a slightly higher da/dN at lower values of ΔK than those tested at lower pressures, but at high ΔK values, da/dN is lower. More work needs to be done to resolve this enigma.

The damage due to hydrogen is very similar for both hydrogen embrittlement (generally monotonic loading) and fatigue (dynamic loading). In the case of hydrogen embrittlement, the deleterious effect of hydrogen roughly corresponds to the strength of the steel. This has been shown by data for reduction of area of smooth tensile specimens, tested in hydrogen relative to those tested in air [6,46,47]. There is also a strong inverse correlation between threshold stress intensity and steel strength, shown by Gangloff [39]. For the case of reduction of area, Fig. 13 shows the difference in reduction of area between tests in air and tests in hydrogen for a number of steels that have a wide range of strength. Included in the figure are data points for the X52 and X100 alloys tested here. They exhibit relatively high differences in reduction of area, but the same trend as other steels, as a function of yield strength. These two alloys show no such correlation between yield strength and fatigue crack growth rate. This is significant, because if fatigue-based design is used, both stronger and thinner steel can be employed, resulting in reduced costs for transportation of hydrogen gas via pipeline. However, the correlation of hydrogen embrittlement increasing as the strain rate is decreased, or in other words, as
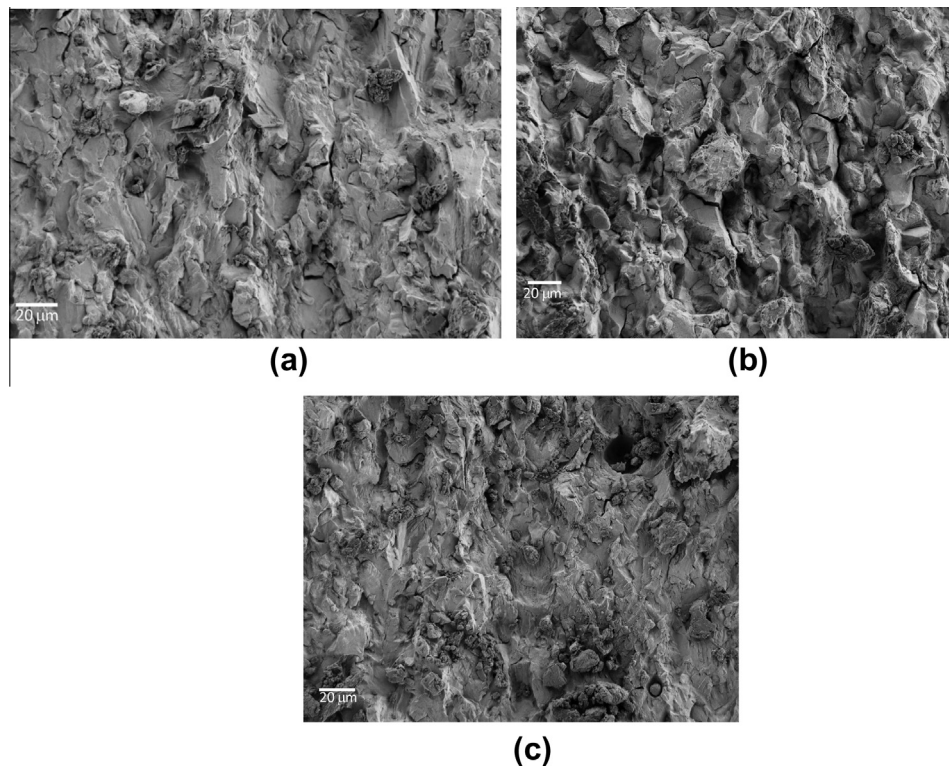
Fig. 10. Fatigue surfaces of X100 steel tested in pressurized (20.7 MPa) hydrogen gas in the following regimes: fatigue precrack (a), transient (b), and steady-state crack growth (c). Region (a) is characterized by mixed intergranular–transgranular fracture that changes to predominantly intergranular fracture with some planar fracture and fatigue striations in region (b), and predominantly transgranular fracture with crack branching in region (c).
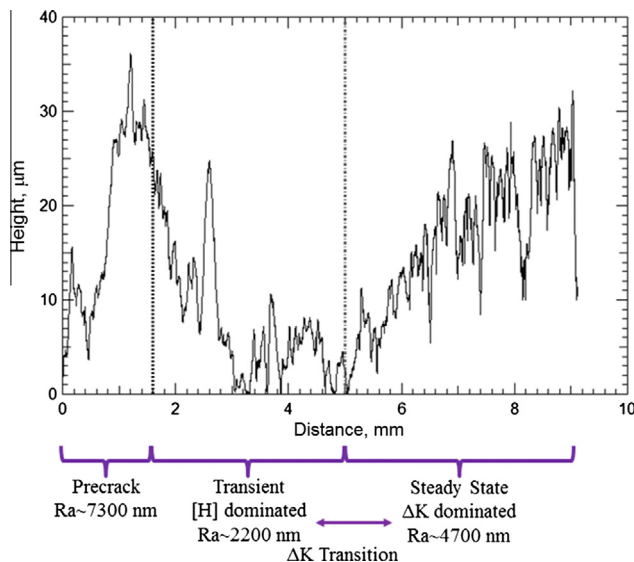

Fig. 11. Profilometry trace of the fatigue surface of X100 steel tested in 20.7 MPa hydrogen. Crack growth was from left to right.

Fig. 12. Stress-assisted-hydrogen-diffusion and relative-plastic-zone sizes for both X52 and X100.

the time for hydrogen diffusion is increased, holds for FCGR [15]. This can be seen in Figs. 6 and 8. In Fig. 6, FCGR increases as pressure increases, similar to how increasing hydrogen, either through gas pressure or increased voltage from cathodic charging, increases hydrogen embrittlement [14,17,44]. In Fig. 8, FCGR increases as cyclic frequency decreases, allowing more time for hydrogen to diffuse to the crack tip, which is commonly seen in the case of hydrogen embrittlement [3–17].

6. Conclusions

For both X100 and X52 the FCGR is one to two orders of magnitude higher in a pressurized hydrogen environment than in air. This enhanced growth rate appears to correlate to pressure for X100 but is not clear for X52. There appears to be little difference between the overall range of FCGRs of X52 and X100, whether in pressurized hydrogen or air. However, both materials, when tested in hydrogen, display a fracture surface which transitions from mostly intergranular to mostly transgranular fracture as the ΔK increases. The FCGR data has a transition, or knee, between ΔK values of 11 MPa m$^{1/2}$ and 15 MPa m$^{1/2}$. Before the transition, crack growth in hydrogen gas is characterized by a slope greater than that in air, probably due to increased hydrogen concentration as

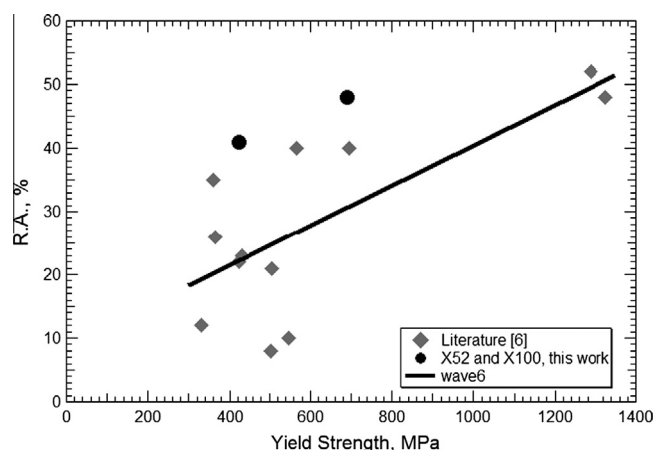**Fig. 13.** Difference in reduction of area, defined as that in air minus that in hydrogen gas, for a number of steels (diamonds) and for the two pipeline steels measured in this work (circles), including a linear trend-line for the steel (diamonds) data, as a function of yield strength [6].

a function of stress-driven hydrogen diffusion to the crack tip. After the transition, the slope of the rate of crack growth as a function of ΔK is similar to that in air, but at a cracking rate 1–2 orders of magnitude higher. Perhaps the hydrogen concentration is saturated in the crack process zone at such high levels of stress intensity.

Acknowledgement

References

[1] Fuel Cell and Hydrogen Energy Association website, June 27, 2013. <http://www.fchea.org/index.php?id=53>.

[2] Department of Transportation website, June 27, 2013. <http://www.phmsa.dot.gov/portal/site/PHMSA/menuitem.ebdc7a8a7e39f2e55cf2031050248a0c/?vgnextoid=2c6924cc45ea4110VgnVCM1000009ed07898RCRD&vgnextchannel=f7280665b91ac010VgnVCM1000008049a8c0RCRD&vgnextfmt=print>.

[3] H.J. Cialone, J.H. Holbrook, Sensitivity of steels to degradation in gaseous hydrogen, Hydrogen Embrittlment: Prevention and Control, Los Angeles, CA, 1985, pp. 134–152.

[4] N.E. Nanninga, A.J. Slifka, Y.S. Levy, C. White, A review of fatigue crack growth for pipeline steels exposed to hydrogen, Journal of Research of the NIST 115 (2010) 1–16.

[5] C. San Marchi, B.P. Somerday, K. Nibur K, D.G. Stalheim, T. Boggess, S. Jansto, Fracture and fatigue of commercial grade API pipeline steels in gaseous hydrogen, in: Proceedings of the ASME 2010 Pressure Vessels & Piping Conference, Bellevue, WA, pp. 1–10.

[6] C. San Marchi, B.P. Somerday, Technical Reference on Hydrogen Compatibility of Materials: Plain Carbon Ferritic Steels: C–Mn alloys (Code 1100), Sandia National Laboratories, October 2010. <http://www.sandia.gov/matlsTechRef/> (accessed 01.03.12).

[7] A. Duncan, P.-S. Lam, T. Adams, Tensile testing of carbon steel in high pressure hydrogen, in: Proceedings of the ASME Pressure Vessels and Piping Conference, San Antonio, TX, 2007, pp. 1–7.

[8] K.A. Nibur, B.P. Somerday, D.K. Balch, C. San Marchi, Sustained load cracking of steels for hydrogen storage and delivery, in: Effects of Hydrogen on Materials, ASM International, Materials Park, OH, 2008, pp. 341–348.

[9] I. Moro, I. Briottet, P. Lemione, E. Andrieu, C. Blanc, G. Odemer, J. Chene, F. Jambon, Damage under high pressure hydrogen environment of a high strength pipeline steel X80, in: Effects of Hydrogen on Materials, ASM International, Materials Park, OH, 2008, pp. 357–364.

[10] K. Xu, M. Rana, Tensile and fracture properties of carbon and low alloy steels in high pressure hydrogen, in: Effects of Hydrogen on Materials, ASM International, Materials Park, OH, 2008, pp. 357–364.

[11] A. Mustapha, E.A. Charles, D. Hardie, Evaluation of environment-assisted cracking susceptibility of a grade X100 pipeline steel, Corrosion Science 54 (2012) 5–9.

[12] P.S. Lam, R.L. Sindelar, T.M. Adams, Literature survey of gaseous hydrogen effects on the mechanical properties of carbon and low alloy steels, in: Proceedings of the ASME 2007 Pressure Vessels & Piping Conference, San Antonio, TX, pp. 501–518.

[13] D.G. Stalheim, T. Boggess, C. San Marchi, S. Jansto, B.P. Somerday, G. Muralidharan, P. Sofronis, Microstructure and mechanical property performance of commercial API pipeline steels in high pressure gaseous hydrogen, in: Proceedings of IPC 2010, 8th International Pipeline Conference, Calgary, Alberta, Canada, IPC2010-31301.

[14] D. Hardie, E.A. Charles, A.H. Lopez, Hydrogen embrittlement of high strength pipeline steels, Corrosion Science 48 (2006) 4378–4385.

[15] J. Toribio, The role of crack tip strain rate in hydrogen assisted cracking, Corrosion Science 39 (9) (1997) 1687–1697.

[16] A.T. Yokobori Jr., Y. Chinda, T. Nemoto, K. Satoh, T. Yamada, The characteristics of hydrogen diffusion and concentration around a crack tip concerned with hydrogen embrittlement, Corrosion Science 44 (2002) 407–424.

[17] N.E. Nanninga, Y.S. Levy, E.S. Drexler, R.T. Condon, A.E. Stevenson, A.J. Slifka, Comparison of hydrogen embrittlement in three pipeline steels in high pressure gaseous hydrogen environments, Corrosion Science 59 (6) (2012) 1–9.

[18] S. Suresh, R.O. Ritchie, Mechanistic dissimilarities between environmentally influenced fatigue-crack propagation at near-threshold and higher growth rates in lower strength steels, Metal Science 16 (1982) 529–538.

[19] R.J. Walter, W.T. Chandler, Cyclic-load crack growth in ASME SA-105 Grade II Steel in high-pressure hydrogen at ambient temperature, in: Effect of Hydrogen on Behavior of Materials Moran, WY, 1976, pp. 273–286.

[20] C. San Marchi, B.P. Somerday, K.A. Nibur, D.G. Stalheim, T. Boggess, S. Jansto, Fracture resistance and fatigue crack growth of X80 pipeline steel in gaseous hydrogen, in: Proceedings of the ASME 2011 Pressure Vessels and Piping Conference, Baltimore, Maryland, PVP2011-57684.

[21] B.T. Lu, J.L. Luo, P.R. Norton, Environmentally assisted cracking mechanism of pipeline steel in near-neutral pH groundwater, Corrosion Science 52 (5) (2010) 1787–1795.

[22] L. Tau, S.L.I. Chan, C.S. Shin, hydrogen enhanced fatigue crack propagation of bainitic and tempered martensitic steels, Corrosion Science 38 (11) (1996) 2049–2060.

[23] J. Capelle, J. Gilgert, G. Pluvinage, A fatigue initiation parameter for gas pipe steel submitted to hydrogen absorption, International Journal of Hydrogen Energy 35 (2010) 833–843.

[24] A. Alhussein, J. Capelle, J. Gilgert, S. Dominiak, Z. Azari, Influence of sandblasting and hydrogen on tensile and fatigue properties of pipeline API 5L X52 steel, International Journal of Hydrogen Energy 36 (2011) 2291–2301.

[25] ASME B31.12-2008, Hydrogen Piping and Pipelines, American Society of Mechanical Engineers, New York, 2009, p. 258.

[26] K. Ichitani, M. Kanno, Visualization of hydrogen diffusion in steels by high sensitivity hydrogen microprint technique, Science and Technology of Advanced Materials 4 (2003) 545–551.

[27] Y. Kim, Y. Kim, D. Kim, S. Kim, W. Nam, H. Choe, Effects of hydrogen diffusion on the mechanical properties of austenite 316L steel at ambient temperature, Materials Transactions 52 (3) (2011) 507–513.

[28] M.H. Marvasti, W. Chen, R.L. Eadie, Fatigue of steel in air a low cyclic loading frequency, Scripta Materialia 64 (2011) 552–555.

[29] S.H. Wang, W. Chen, A study of pre-cyclic-load-induced burst of creep deformation of a pipeline steel under subsequent static load, Materials Science and Engineering A A325 (2002) 144–151.

[30] ASTM E8-04, Standard test method for tension testing of metallic materials, ASTM International, West Conshohocken, PA, 2005, p. 24.

[31] ASTM E647-05, Standard test method for measurement of fatigue crack growth rates, ASTM International, West Conshohocken, PA, 2005, p. 45.

[32] ASTM E399-06, Standard test method for linear-elastic plane-strain fracture toughness K_{Ic} of metallic materials, ASTM International, West Conshohocken, PA, 2007, p. 3.

[33] J. Keller, B.P. Somerday, C. San Marchi, Hydrogen embrittlement of structural steels, FY 2011 Annual Progress Report, DOE Hydrogen and Fuel Cells Program, 2012, pp. 299–302.

[34] R.L. Amaro, N. Rustagi, K.O. Findley, E.S. Drexler, A.J. Slifka, Modeling the fatigue crack growth of X100 pipeline steel in gaseous hydrogen, International Journal of Fatigue (8) (2013). <http://www.sciencedirect.com/science/article/pii/S0142112313002259> (accessed 19.09.13).

[35] R.P. Gangloff, Hydrogen assisted cracking in high strength alloys, in: comprehensive structural integrity, in: I. Milne, R.O. Richie, O. Karihaloo, J. Petit, P. Scott (Eds.), Comprehensive Structural Integrity, vol. 6, Elsevier Science, New York, NY, 2003.

[36] C.J. McMahon Jr., X. Liu, J. Kameda, M.C. Morgan, Recent observation of hydrogen-induced cracking of high-strength steels, in: Effects of Hydrogen on Materials, ASM International, Materials Park, OH, 2008, pp. 46–53.

[37] I.M. Austen, P. McIntyre, Corrosion fatigue of high-strength steel in low-pressure hydrogen gas, Metal Science 13 (7) (1979) 420–428.

[38] R.P. Wei, G.W. Simmons, Environment enhanced fatigue crack growth in high-strength steels, in: Stress Corrosion Cracking and Hydrogen Embrittlement of Iron Base Alloys, Unieux-Firminy, France, 1973, pp. 751–765.

[39] R.P. Gangloff, Science-based prognosis to manage structural alloy performance in hydrogen, in: Effects of Hydrogen on Materials, ASM International, Materials Park, OH, 2008, pp. 1–21.

[40] R.P. Gangloff, Hydrogen assisted cracking of high strength alloys, in: I. Milne, R.O. Ritchie, B. Karihaloo (Eds.), Comprehensive Structural Integrity, vol. 6, Elsevier Science, New York, NY, 2003, pp. 31–101.

[41] M. Gao, R.P. Wei, A hydrogen partitioning model for hydrogen assisted crack growth, Metallurgical Transactions A 16 (11) (1985) 2039–2050.

[42] J.P. Thomas, R.P. Wei, Corrosion fatigue crack growth of steels in aqueous solutions I: experimental results and modeling the effects of frequency and temperature, Materials Science and Engineering A A159 (2) (1992) 205–221.

[43] J.P. Thomas, R.P. Wei, Corrosion fatigue crack growth of steels in aqueous solutions II: modeling the effects of DK, Materials Science and Engineering A A159 (2) (1992) 223–229.

[44] J. Capelle, I. Dmytrakh, G. Pluvinage, Comparative assessment of electrochemical hydrogen absorption by pipeline steels with different strength, Corrosion Science 52 (2010) 1554–1559.

[45] I.M. Dmytrakh, O.D. Smiyan, A.M. Syrotyuk, O.L. Bilyy, Relationship between fatigue crack growth behaviour and local hydrogen concentration near crack tip in pipeline steel, International Journal of Fatigue 50 (2013) 26–32.

[46] J.H. Holbrook, E.W. Collings, H.J. Cialone, E.J. Drauglis, Hydrogen Degradation of Pipeline Steels: Final Report, Brookhaven National laboratory, BNL-52049, March 1986, p. 92.

[47] R.P. Jewett, R.J. Wlater, W.T. Chandler, R.P. Frohmberg, Hydrogen Environment Embrittlement of Metals, NASA, NASA CR-2163, March 1973, pp. 58–61.